AIAA 2002-2744

Discrete Roughness Effects on Shuttle Orbiter at Mach 6

Scott A. Berry and H. Harris Hamilton II

NASA Langley Research Center,
Hampton, VA 23681

32nd AIAA Fluid Dynamics Conference

June 24-27, 2002 / St. Louis, MO

Discrete Roughness Effects on Shuttle Orbiter at Mach 6

By
Scott A. Berry* and H. Harris Hamilton II†
NASA Langley Research Center

Abstract

Discrete roughness boundary layer transition results on a Shuttle Orbiter model in the NASA Langley Research Center 20-Inch Mach 6 Air Tunnel have been reanalyzed with new boundary layer calculations to provide consistency for comparison to other published results. The experimental results were previously obtained utilizing the phosphor thermography system to monitor the status of the boundary layer via global heat transfer images of the Orbiter windward surface. The size and location of discrete roughness elements were systematically varied along the centerline of the 0.0075-scale model at an angle of attack of 40 deg and the boundary layer response recorded. Various correlative approaches were attempted, with the roughness transition correlations based on edge properties providing the most reliable results. When a consistent computational method is used to compute edge conditions, transition datasets for different configurations at several angles of attack have been shown to collapse to a well-behaved correlation.

Nomenclature

M	Mach number
Re	unit Reynolds number (1/ft.)
Re_L	length Reynolds number based on L
p	pressure (psi)
T	temperature (°R)
x	longitudinal distance from the nose (in)
L	model reference length from nose to body-flap hinge line (9.7 in)
k	roughness element height (in)
α	model angle of attack (deg)
δ	boundary layer thickness (in)
θ	momentum thickness (in)
Re_θ	momentum thickness Reynolds number
Re_k	roughness Reynolds number based on height k and conditions at k
Re_{ke}	roughness Reynolds number based on height k and edge conditions
h	heat transfer coefficient (lbm/ft^2-sec) $= q/(H_{aw} - H_w)$ where $H_{aw} = H_{t2}$
h_{F-R}	reference coefficient using Fay-Ridell calculation to stagnation point of a sphere
q	heat transfer rate (BTU/ft^2-sec)
H	enthalpy (BTU/lbm)

Subscripts

∞	freestream static conditions
t1	reservoir conditions
t2	stagnation conditions behind normal shock
e	local edge condition
aw	adiabatic wall
w	model surface
tr	transition onset
inc	incipient
eff	effective

Introduction

The Space Shuttle Orbiter represents the current state-of-the-art in reusable launch vehicles (RLV), despite the fact that it was designed and built over 25 years ago, and it remains the only viable reusable launch platform for the at least the next decade. Recent attempts at designing the next-generation RLV (for instance, the X-33 single-stage-to-orbit (SSTO) concept) have resulted in optimistic design concepts that have not been supported by either the level of technological readiness or the availability of funds to mature the readiness levels sufficiently. While a SSTO represents a significant advancement in the state of the art, more recent designs associated with the Space Launch Initiative (SLI) have returned to two-stage-to-orbit (TSTO) concepts that appear more technologically feasible. A restructuring of NASA's RLV design efforts under the SLI program has resulted in delayed milestones with a decision to proceed to full-scale development of the next-generation RLV in 2006 and replacement of the aging Orbiter fleet by 2012. The Orbiter, therefore, is likely to be the only vehicle available in the near term to obtain valuable aerothermodynamic (more specifically, boundary layer transition) flight data that can be used to minimize design uncertainties for the next-generation RLV.

* Aerospace Engineer, Aerothermodynamics Branch, Aerodynamics, Aerothermodynamics, and Acoustics Competency.
† Adjunct Professor, North Carolina State University, Member AIAA.

Early in the design process of the Space Shuttle Orbiter, boundary layer transition was recognized as one of the major aerothermodynamic challenges to be addressed through extensive ground-based testing.[1] The aerothermodynamic database that was developed prior to the first flight of the Orbiter in 1981 resulted from over 12 years of testing in many of the major U.S. ground-based facilities. This database development was prior to the availability of computational fluid dynamics (CFD) capabilities. Consequently, wind tunnels were heavily utilized to define the boundary layer transition criteria that would predict when during reentry the vehicle would transition from laminar to turbulent flow. The resulting wind tunnel derived transition criteria were thought to be conservative (due to the influence of tunnel-noise contamination associated with conventional facilities) and this was validated when the Orbiter eventually flew.[1] However, the Orbiter occasionally experiences boundary layer transition earlier than nominal due to surface roughnesses[2] that result from the relatively fragile nature of the thermal protection system (TPS) ceramic tiles. The Orbiter typically suffers launched-induced damage to the TPS (gouges in the tiles from ice debris falling off the tank at lift-off) and occasional protrusions of the tile gap fillers that lead to early transition during the reentry. The random nature of this roughness, unfortunately, allows for a wide range of free-stream conditions (Mach numbers between 6 and 18 and length Reynolds numbers between 2.5 and 13 million) at which transition occurs in flight. The conservative design philosophy that was utilized for the Orbiter has compensated for the occasional early transition results thus far. However, for next-generation RLV's where design margins will need to be reduced to enhance payload capability, this amount of scatter does little to promote confidence for reliable transition prediction.

To help reduce uncertainties associated with hypersonic boundary layer transition, a study of roughness effects on the Orbiter has been on-going at NASA Langley Research Center (LaRC) in hopes of developing a better predictor of transition behavior. A ground-based investigation of roughness-induced transition on the Shuttle Orbiter was conducted at LaRC, and the results were subsequently published in Refs. 3 and 4. The two-color relative-intensity phosphor thermography system was used to obtain global heat transfer images of a 0.0075-scale Orbiter windward surface in the LaRC 20-Inch Mach 6 Air Tunnel. Discrete roughness elements were systematically placed along the windward centerline and the model tested over a wide range of unit Reynolds number for an angle of attack of 40 deg. The resulting transition data had shown that a simple approach for correlating roughness transition data utilizing the momentum thickness Reynolds number divided by the edge Mach number (Re_θ/M_e) and the boundary layer trip height divided by the boundary layer thickness (k/δ) seemed to accurately predict when transition would occur. As the study was originally part of a larger effort being coordinated by the NASA Johnson Space Flight Center (JSC), the boundary layer parameters were provided by JSC using the BLIMP[5] code. All the data, from wind tunnels at LaRC and AEDC, as well as flight, were compared based on boundary-layer parameters computed from this same code.[4] Since then, additional boundary layer transition studies for the X–33[6] and X–38[7] programs were conducted at LaRC utilizing this same experimental approach but with LATCH[8] calculations for the boundary layer parameters. While the wind tunnel transition results from the X-33 and X-38 studies were also well correlated by the Re_θ/M_e vs. k/δ approach, the results did not agree with the Orbiter correlation built on BLIMP calculations. Figure 1 provides a comparison of the published transition results from the Orbiter and X-33 studies, which disagree by almost a factor of two. The present paper will investigate this disagreement by reanalyzing the Orbiter results with a consistent computational method for comparison to the X-33 and X-38 published results.

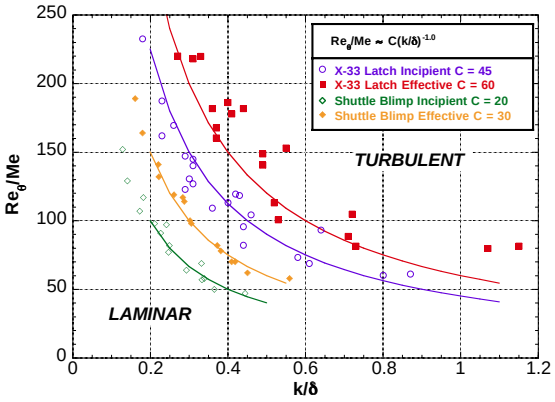

Fig. 1 Comparison of published Orbiter (Ref 3) and X-33 (Ref. 6) results

A recent review of roughness-dominated transition correlations[9] has stated as its goal a reanalysis of recently published results in an attempt to unify the correlating approach. While

certainly a worthy endeavor, this paper did not acknowledge the critical importance of the computational methods used within the different datasets that were being compared. Uncertainties in flowfield calculations associated with a transition study will directly influence the uncertainty of the correlation method.[10] Different computational methods can provide significant differences in the calculated edge properties used to form the correlations, as noted in Refs. 11 and 12. Relevant to the present paper, Ref. 9 compared the published Orbiter[3,4] and X-33[6] results, which were (as discussed earlier) based on different codes. The present investigation, therefore, compares the Orbiter and X-33 results once consistent computations are obtained. In summary, the objectives of this paper are to investigate the influence of the computational method on the development of discrete roughness correlations, to compare various roughness-dominated transition datasets that are based on a consistent approach, and to examine alternate correlation approaches. The Orbiter experimental roughness transition data utilized here was previously published in Ref. 3, although new smooth model results are included.

Transition Correlations

Hypersonic boundary layer transition became relevant with the dawning of the era of ballistic reentry vehicles in the mid-1950s.[10] Over the years hypersonic vehicle concepts have changed dramatically, starting with the blunt ballistic vehicles, then the moderately-blunt lifting bodies, and recently the slender air-breathing configurations. The approaches that different researchers have used over the years to correlate empirically derived transition results have also changed. However, during the last 50 or so years of research, no universal transition correlation method has yet to be identified that can predict transition in flight for all classes of vehicles.

Initially, researchers focused on blunt reentry vehicles, and in particular the problem of nosetip transition. There are many references available (far too numerous to site all) that discuss the importance of surface roughness in the subsonic portion of the nosecone. Reference 13 provides an overview of much of the early work on nosetip transition and in particular the large database provided by the Passive Nosetip Technology (PANT) program. A large majority of this work focused on the problem of distributed surface roughness that develops from ablating nosecones. The surface ablation, which usually is driven by the early laminar conditions, causes the formation of micro roughness patterns that are dependent upon the material composition and fabrication process. This work has led to the concept of the critical roughness Reynolds number (Re_k) approach for blunt bodies in hypersonic flow.[9] This approach requires detailed computations of the flowfield within the boundary layer, as Re_k is calculated based on local condition at the trip height. Because of the difficulty in obtaining high-quality boundary-layer profile data for a wide range of flow conditions, many researchers have simplified this approach by using edge conditions instead of the trip height to calculate the local Reynolds number to provide an Re_{ke} (for instance, see Ref. 14).

Since the early 1980s, research efforts have shifted to moderately blunt lifting-body vehicles, like the Shuttle Orbiter. Boundary layer transition on these vehicles tends to occur at a point on the body where the boundary layer edge is mostly supersonic. For the Orbiter, much of the transition database that was obtained prior to the first flight was to define the distributed surface roughness limit for the vehicle that would allow it to still be considered "aerothermodynamically smooth." Based on the Orbiter design philosophy, a smooth surface was defined as a surface whose roughness did not promote transition any earlier than what was predicted based on conservative wind tunnel derived correlations.[1] An average distributed roughness on the order of 0.05-in for the full-scale Orbiter appears to represent a smooth vehicle, based on post-flight analysis.[2] The remainder of the Orbiter transition database was dedicated to understanding the effect of isolated (discrete) three-dimensional roughness elements that exceed the distributed roughness limit. Van Driest and Blumer[14] developed an effective roughness transition correlation based on edge conditions using spherical trips on a sharp cone in a supersonic wind tunnel. This correlation appeared to correctly predict transition onset near the Orbiter nose based on post-flight analysis of the STS-1 to 5 flights. On flights where transition occurred significantly early due to protruding gap fillers (STS-28 and 73, for instance), the estimated roughness heights in flight[2] exceeded the minimum required effective height based on the Van Driest and Blumer correlation. (Unfortunately, the actual dimensions of the protruding gap fillers are not known during the flight, but must be estimated based on post-flight inspections.) For future lifting-body RLV designs

(Orbiter-like configurations), if the distributed surface roughness can be minimized, transition behavior in flight will most likely be influenced by discrete roughness elements.

To investigate different transition correlations, appropriate boundary layer parameters must be obtained for comparison. Reference 15 provides a substantial, but not exhaustive, list of possible transition correlations to evaluate. To attempt to look at all these correlations would be a monumental undertaking. The present paper will judiciously select a moderate subset (necessarily influenced by the parameters available from the choice of computational method) of the transition correlation approaches that have been attempted over the past 50 years. As noted in Ref. 9, a power-law relationship between an assumed disturbance parameter (usually related to the roughness height) and an assumed transition parameter (usually related to the local conditions within the calculated laminar boundary layer) is typically sought. A lot of the Orbiter work has been based on the selection of Re_θ/M_e as the transition parameter.[1] Also, the disturbance parameter has typically been based on the trip height referenced by boundary-layer edge properties (boundary layer or momentum thickness) or by Re_k.

The flowfield properties that are used to develop the parameters for the correlations can be obtained from computational methods of differing complexity and sophistication. The simplest methods to implement are based on engineering codes (for example, Miniver[16]), which, typically, provide boundary layer edge properties, but not the properties within the boundary layer that are required to formulate the Re_k parameter. More sophisticated codes that solve the differential form of the boundary layer equations are required to obtain Re_k values, however at the expense of additional computational time and resources. Viscous Navier-Stokes solutions could also provide all the necessary properties, but with the added complexity of grid sensitivity issues associated with the proper derivation of the boundary layer edge.[10]

Experimental Method

Test Facility

The present experimental discrete roughness results, originally published in Ref. 3, were obtained in the LaRC 20-Inch Mach 6 Air Tunnel. Miller (Ref. 17) provides a detailed description of this hypersonic blowdown facility, which uses heated, dried, and filtered air as the test gas. Typical operating conditions for the tunnel are stagnation pressures ranging from 30 to 500 psia, stagnation temperatures from 760 to 940-degR, and freestream unit Reynolds numbers from 0.5 to 8 million per foot. A two-dimensional, contoured nozzle is used to provide nominal freestream Mach numbers from 5.8 to 6.1. The test section is 20.5 by 20 inches; the nozzle throat is 0.399 by 20.5-inch. A bottom-mounted model injection system can insert models from a sheltered position to the tunnel centerline in less than 0.5-sec. Run times up to 15 minutes are possible with this facility, although for the current heat transfer and flow visualization tests, the model was exposed to the flow for only a few seconds. Flow conditions were determined from the measured reservoir pressure and temperature and the measured pitot pressure at the test section and were compared to a recent unpublished calibration of the facility.

Test Techniques

The two-color relative-intensity phosphor thermography technique is now routinely being applied to aeroheating tests in the hypersonic wind tunnels of LaRC. Details of the phosphor thermography technique are provided in Refs. 18, 19, and 20. References 3, 6, and 7 are recent examples of the application of this technique to wind tunnel testing. The primary advantage of phosphor thermography is the global resolution of the quantitative heat transfer data. Such data can be used to identify the heating footprint of complex, three-dimensional flow phenomena (e.g., transition fronts, turbulent wedges, boundary layer vortices, etc.) that are extremely difficult to resolve by discrete measurement techniques. Phosphor thermography is routinely used in Langley's hypersonic facilities as quantitative global surface heating information is obtained from models that can be fabricated quickly (a few weeks) and economically (an order of magnitude less than the thin-film technique). Recent comparisons of heat transfer measurements obtained from phosphor thermography to conventional thin-film resistance gauges measurements (Ref. 21) and CFD predictions (Ref. 22, and 23) have shown excellent agreement.

Model Description

Cast ceramic models of 0.0075-scale Shuttle Orbiter were built in accordance with the procedures detailed in Ref. 24. The models were

then coated with a mixture of phosphors suspended in a silica-based colloidal binder. This coating consisted of a 5:1 mixture of lanthanum oxysulfide (La_2O_2S) doped with trivalent europium and zinc cadmium sulfide (ZnCdS) doped with silver and nickel in a proprietary ratio. The coatings typically do not require refurbishment between runs in the wind tunnel and have been measured to be approximately 0.001 inches thick. The final step in the fabrication process is to apply fiducial marks along the body to assist in determining spatial locations accurately. The fiducial marks used for this investigation were selected to correspond to the roughness element locations and, as noted in Ref. 3, were identical to the trip locations used in Ref. 25 with the exception of additional centerline locations at DE and ECL. Table 1 provides a list of the fiducial marks used for the present investigation, while Fig. 2 provides a sketch of these trip locations, and shows details of the trip dimensions.

The roughness elements as fabricated, simulate a raised TPS tile, as discussed in Ref. 3. The trips were cut from 0.0025-inch thick polyimide tape and variations on the roughness heights (k) were obtained by stacking multiple layers of tape (heights of 0.0025, 0.005, 0.0075, and 0.010-inch were used). Roughness elements fabricated from the tape were easily applied to the trip locations and removed without adversely affecting the phosphor coating. The trip designation used for the present study utilizes the station name followed by the number of layers (for instance, B2 identifies a 0.005-in trip at station B).

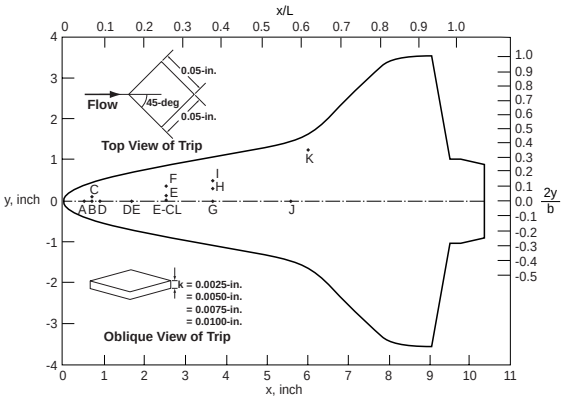

Fig. 2 Sketch of 0.0075-scale Orbiter windward surface showing fiducial mark locations and details of the trips.

Test Conditions

The LaRC 20-Inch Mach 6 Air Tunnel provides a freestream unit Reynolds number (Re) variation of 0.5 to 8.0 million per foot. For a 0.0075-scale model, this corresponds to a length Reynolds number (Re_L) of approximately 0.4 to 6.7 million. The upper bound of the wind tunnel range is within in the general range of Re_L in flight at the time of transition.[2] To obtain roughness transition data, the unit Reynolds number was systematically varied for each trip height and location to obtain the incipient, critical, and effective Reynolds numbers. Note that the present terminology is similar to the definitions of Bertin[26] except that the terms are a function of Reynolds number instead of trip height. Van Driest and Blumer,[14] Boudreau,[27] and Pate[28] discuss trip effectiveness as a function of Re, but without the use of these specific terms. And while Boudreau defined effectiveness based on the end of transition, transition onset is used for the present study (in the tradition of Bertin). The incipient Reynolds number was identified, based on the heating distributions, by the maximum Reynolds number at which laminar flow was maintained behind the trip. The critical Reynolds number corresponds to the Re where significant non-laminar flow first appears downstream of the roughness element. The effective Reynolds number was identified by the minimum Re where the transition front appears fixed at or near the roughness element. Generally, the Re increment from run to run was on the order of 0.5 million per foot. Typically, the incipient, critical, and effective values of Re would be identified within three incremental runs in the tunnel. The sideslip was maintained at zero for all the runs presented herein.

Data Reduction

Heating rates were calculated from the global surface temperature measurements using one-dimensional semi-infinite solid heat-conduction equations, as discussed in detail in Refs. 18 and 19. Based on considerations presented in Ref. 18, phosphor system measurement error is believed to be less than ±8%, with overall experimental uncertainty of ±15%. Heating distributions are presented in terms of the ratio of heat-transfer coefficients $h/h_{F\text{-}R}$, where $h_{F\text{-}R}$ corresponds to the Fay and Ridell[29] stagnation-point heating to a sphere with radius 0.09-in (a one-foot radius sphere scaled to the model size). Repeatability of the centerline heat transfer distributions was found to be generally better than ±4%. The IHEAT data reduction program discussed in Ref. 18 was used to accurately extract the heating distributions along the model centerline.

Computational Methods

Edge Conditions

The engineering code LATCH (Langley Approximate Three-Dimensional Convective Heating)[8] was used to obtain the boundary-layer edge properties for the present paper. This approximate method for calculating heating rates on three-dimensional bodies has been validated against both experimental and computational results. LATCH is based on the axisymmetric analog for three-dimensional boundary layers and uses a generalized body-fitted coordinate system to compute edge properties and heating along individual streamlines. Edge conditions for the boundary-layer solution are obtained along the streamlines from an inviscid flowfield calculated by an inviscid version of the LAURA code.[30] Further details in regards to the LATCH code can be found in Ref. 8.

For approximate methods, the classical approach of assuming that the boundary layer edge properties are given by the inviscid wall conditions has been shown to be inappropriate for blunt bodies.[31] Within LATCH, the boundary-layer edge properties can be obtained by interpolating in the inviscid flowfield a distance equal to the boundary-layer thickness away from the wall. To accomplish this, an initial assumption is made for the boundary-layer edge properties (usually the wall values), and the boundary-layer thickness is computed. Then the edge properties are re-computed based on this new location within the flowfield and the solution is iterated until the re-computed boundary-layer thickness is equal to the assumed value. This process usually takes two or three iterations to converge. The use of edge properties determined in this manner approximately accounts for the effect of variable entropy at the boundary-layer edge. Recent experience with moderately blunt bodies like the Orbiter, however, has shown that based on the inviscid solutions available, iterating away from the surface has a minimal affect on the convective heating solutions (the primary motivation for the code), even though it provides for more exact edge conditions. By assuming the boundary-layer edge properties to be equal to the inviscid surface conditions, which corresponds to a constant entropy condition, solutions are obtained much quicker. For the present results, therefore, the edge conditions are actually the wall conditions based on the inviscid solution. Results based on a constant entropy assumption will allow for a consistent comparison of the final correlation results to the X-33[6] and X-38[7] results. The LATCH code was utilized to obtain the boundary-layer edge properties for the transition correlations based on the nominal unit Reynolds number (*Re*) cases listed in Table 2. For the case where incipient and effective transition is observed to occur at a *Re* that is between these nominal cases, the transition parameters are interpolated.

Boundary-Layer Profiles

In order to look at other correlating approaches, such as those recommended in Ref. 9, the SABLE code[32] had to be implemented to calculate the boundary-layer profile information not provided by LATCH. The SABLE code is a finite-difference technique that solves the steady, compressible, axisymmetric boundary-layer equations for both laminar and turbulent flows and has been validated against experimental and computational results. Also, the SABLE solutions, which approximately account for the variable entropy condition, have also been used to provide boundary-layer edge properties, based on 99.5% of the edge velocity, for comparison to LATCH.

Comparisons to BLIMP

The boundary-layer correlations developed for the present paper are based solely on these LATCH and SABLE solutions. A comparison of the results from these codes to what had previously been obtained from the BLIMP code in terms of both the transition and disturbance parameters will highlight some important differences. This paper does not intend to imply which code correctly calculates the flowfield properties, only that significant differences can be obtained based on the underlying assumptions within each code.

For the transition parameter Re_θ/M_e, LATCH calculates the local Reynolds number, the momentum thickness and edge Mach number directly. Figure 3 is a comparison of the calculated M_e distributions from LATCH, SABLE, and BLIMP for a representative unit Reynolds number case (Re = 2.73x10^6/ft). For the LATCH solution (representing the constant entropy condition), M_e is significantly lower (consistently 20%) than the BLIMP results (variable entropy). When variable entropy conditions are obtained from the SABLE solutions, M_e is closer to the BLIMP results. The momentum thickness distributions are shown in Fig. 4. In this case, the LATCH results are roughly 20% higher than BLIMP. The variable entropy

result from SABLE, however, nearly matches the BLIMP calculations. The differences in the local edge properties appear to be a result of the entropy condition between the LATCH and BLIMP results and are significant enough to raise concerns about trying to compare correlations based on the different computational methods. Fortuitously, when these edge properties are used to compute Re_θ/M_e most of the differences roughly cancel out, as shown in Fig. 5. The LATCH result is nearly within 10% of BLIMP, while the SABLE result is almost identical. Even though these computational methods provided significant differences in the edge properties, the transition parameter calculation is actually in fairly good agreement. In this case, the difference in the transition parameter between LATCH and BLIMP is less than 15%. The Re_θ/M_e transition parameter appears fairly insensitive to edge property differences, although how applicable, in general, this observation is to other geometries and computational methods is not known.

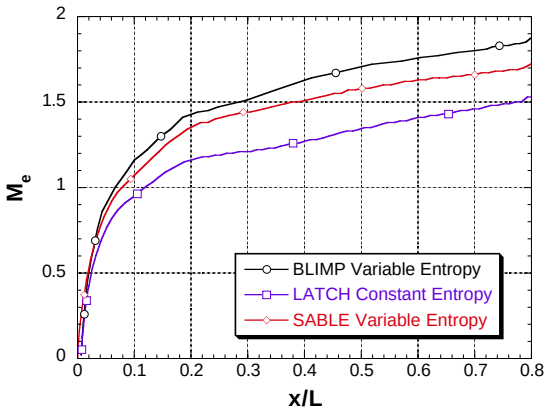

Fig. 3 Comparison of calculated edge Mach number distributions

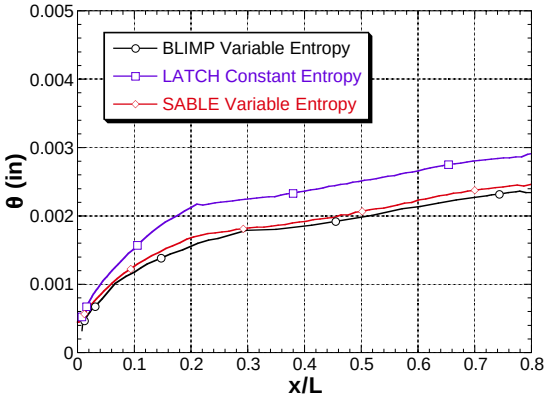

Fig. 4 Comparison of calculated momentum thickness distributions

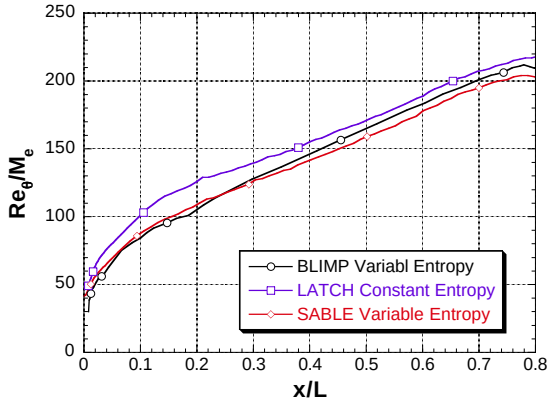

Fig. 5 Comparison of calculated momentum thickness Reynolds number divided by the edge Mach number

For the disturbance parameter k/δ, the trip height (k) is known from the experiment, while the boundary layer thickness (δ) is calculated. In the case of BLIMP, δ is calculated as a direct solution of the boundary layer equations and is based on matching 100% of the edge velocity. Within LATCH, engineering relations[33] are used to obtain both θ and δ, where θ is calculated based on local properties and δ is determined based on the shape factor relation of δ/θ=5.5. The fact that BLIMP computes δ directly while LATCH does not introduces another potential source of error when trying to compare correlations built on different codes. Figure 6 provides a comparison of the boundary layer thickness computed between the codes for the same representative *Re* case discussed earlier. In this case, the SABLE result is in fairly close agreement with LATCH, which is a little surprising considering the differing assumptions and methodologies used. However, the difference between the SABLE and BLIMP results may be more significant. Since SABLE calculates δ based on 99.5% of the edge velocity, while BLIMP uses 100%, much of the differences observed in Fig. 6 might be expected. Based on a typical boundary layer profile obtained from BLIMP, the difference between matching 99.5 and 100% of the edge velocity accounted for nearly a 40% difference in the edge of the boundary layer. As for the comparison between BLIMP and LATCH, the boundary layer thickness from BLIMP is over 50% larger than LATCH. The difference in the calculated boundary layer thickness between the two codes appears to be the major contributing factor to the discrepancy discussed earlier and shown in Fig. 1.

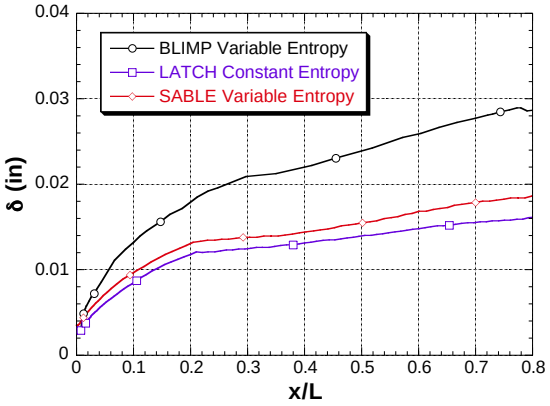

Fig. 6 Comparison of calculated boundary-layer thickness distributions

For disturbance parameters based on Re_k, the SABLE code was used to obtain the flowfield properties within the boundary layer. The distribution of Re_k down the model centerline based on fixed heights within the boundary layer (corresponding to the first three trip heights, k = 0.0025, 0.0050, 0.0075-in, only) from SABLE and BLIMP for the representative unit Reynolds number case (Re = 2.73x10^6/ft) is shown in Fig. 7. The Re_k values from BLIMP are roughly 30% higher than those from SABLE. Since the boundary layer thickness results from BLIMP are much larger than the SABLE results, a steeper velocity profile would be required in order for the Re_k values from BLIMP to be larger than SABLE for fixed heights within the boundary layer. Although the exact reason for the different Re_k results is not known at this time, nevertheless, these differences provides further evidence of the importance of using a consistent computational method when comparing results.

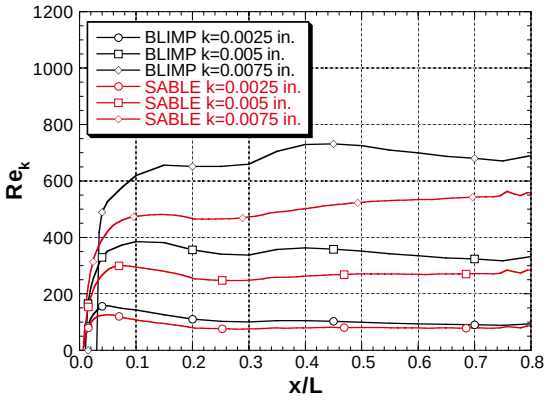

Fig. 7 Comparison of calculated roughness-height Reynolds number distributions

Discussion of Results

A study of roughness-induced boundary-layer transition on the Shuttle Orbiter was completed in the LaRC 20-Inch Mach 6 Air Tunnel and representative heating images and distributions were reported in Ref. 3. The roughness transition results were obtained for a fixed angle of attack (α) of 40-deg. For tests in hypersonic facilities, the preferred method for detecting boundary layer transition, both the beginning and end, is to monitor the surface heat-transfer distributions.[28] Figure 8 provides a comparison of measured centerline heating distributions for a range of Re for the smooth model and for a sample trip case, and are compared to the laminar LATCH heating predictions. These results were newly acquired in the Mach 6 facility. Note the excellent agreement of the non-tripped results for the first half of the model with the laminar computations and the systematic forward movement of natural transition as Re is increased. For the tripped case (Re = 7.9x10^6/ft), the non-laminar heating level quickly reaches a plateau that eventually matches (near the aft end of the model) with the non-laminar heating level for the same Re case without a trip, suggesting that turbulent heating levels have been reached. Figure 9 provides a comparison of the heating images obtained for Re = 7.8x10^6/ft, both with and without trips. For the tripped case, an array of 5 trips (k = 0.0025-in.) across the x/L = 0.258 station at trip stations ECL and E, F, (port and starboard) was used, as can be seen in Fig. 9b. Note the symmetry of the tripped flow and extent of the turbulent flow coverage over 3/4 of the windward surface.

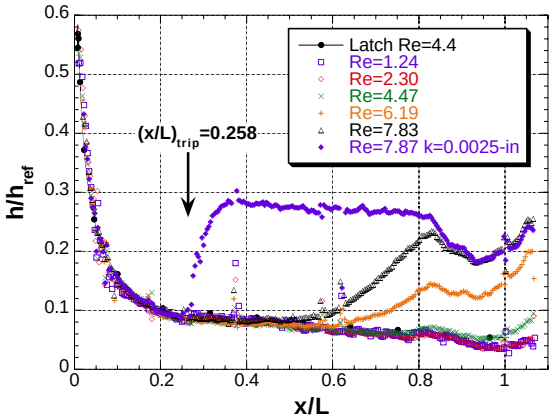

Fig. 8 Comparison of smooth-body and tripped heating distributions for a range of Re to laminar LATCH prediction

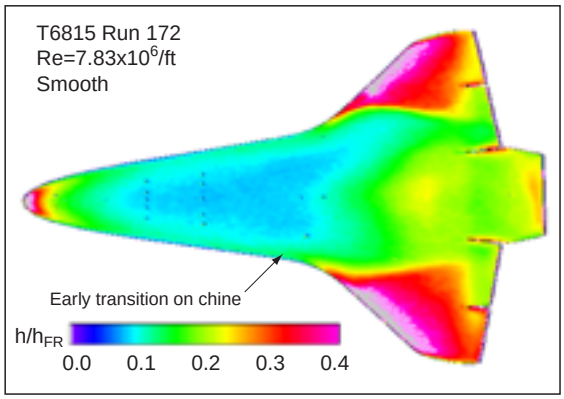

a) Smooth model

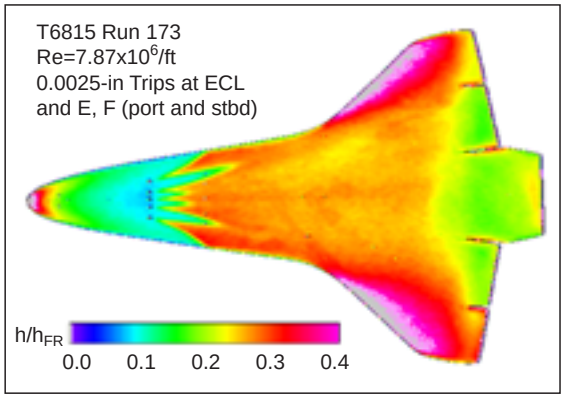

b) 0.0025-in trips at ECL, E, and F (port and starboard)

Fig. 9 Comparison of smooth-body and tripped heating images for $Re = 7.8\text{x}10^6$/ft

Based on the LATCH calculations, the onset of natural transition at $x/L = 0.61$ for $Re = 6.2\text{x}10^6$/ft corresponds to Re_θ/M_e of roughly 290 and δ of 0.010-in. The phosphor surface distributed roughness has recently been measured to be on the order of 0.0005-in nominally, with occasional isolated peaks on the order of 0.0015-in. A close-up inspection of the model surface is typically done prior to testing. By shining a flashlight along the phosphor coating, the larger peaks are identified by the shadows they produce. When peaks are found, a sharp knife is used to carefully remove the peaks without damaging the local phosphor coating. If the pre-test inspection fails to locate all the peaks, smooth model runs at the highest Re condition will illuminate the remaining peaks via disturbances that appear in the phosphor images. Figure 9a is an example of a high-*Re* smooth-model image, where tiny imperfections near the leading edge of the chine produces a small transition wedge that brings transition onset forward on the lower half of the image, thereby making transition appear slightly asymmetric. On centerline, however, there were no indications of the large peaks either from the visual inspection or the heating images. Therefore, the smooth model Re_θ/M_e value of 290 is believed to correspond to a distributed surface roughness to boundary layer height ratio (k/δ) of 0.05. The smallest discrete roughness element (k=0.0025-in) is five times larger than the nominal background roughness and appears fully effective for $Re = 7.8\text{x}10^6$/ft, as shown in Fig. 9b.

Transition Maps

The transition results published in Ref. 3 were systematic and well behaved. To illustrate the transition onset trends, without repeating the data shown in Ref. 3, the location for transition onset, as identified from the heating distribution plots, were plotted as a function of the unit Reynolds number for each trip station. A similar approach has been reported in Refs. 14, 27, and 28. The resulting transition onset maps are shown in Fig. 10. The data presented in these figures represents the results from 5 trip stations along the model centerline, up to 4 trip heights at each station, and a minimum of 5 *Re* for each case, for roughly 100 individual runs in the facility. Each data point shown in Fig. 10 represents the result of a run. For each Re case, the resulting $(x/L)_{tr}$ denotes whether the data indicated laminar, transitional or fully turbulent flow downstream of the trip. For instance, a $(x/L)_{tr}$ value of 1 indicates that the trip had no effect (laminar), a value corresponding to the trip location indicates a fully effective trip, while any value in between represents a critical case. Previous studies[14,27,28] have shown that the curve representing the movement of transition as a function of *Re* is fairly smooth and shows a distinctive sharp bend that represents the effective point. As shown in Fig. 10, the unit Reynolds number increment is too coarse to use a straight line between the data points to represent the transition behavior and, in particular, to isolate an effective value for the correlations to follow. Therefore, a smooth curve fit through the data was used in lieu of straight lines in order to systematically define the bend in the curve that represents the effective point. For each trip case, the smooth curve was placed in a position that allowed the data points to fall within ±10% of the curve. The incipient and effective results obtained from Fig. 10 are tabulated in Tables 3 and 4, respectively, along with the corresponding calculated transition parameters.

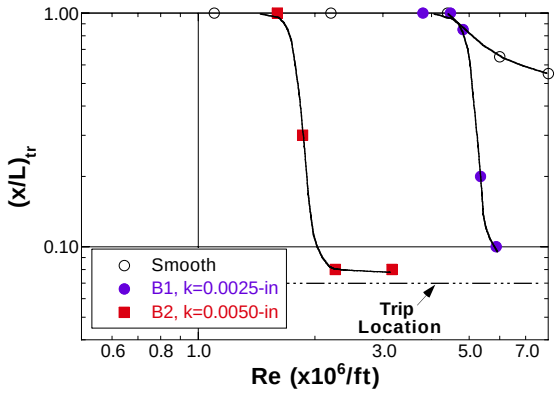

a) Station B

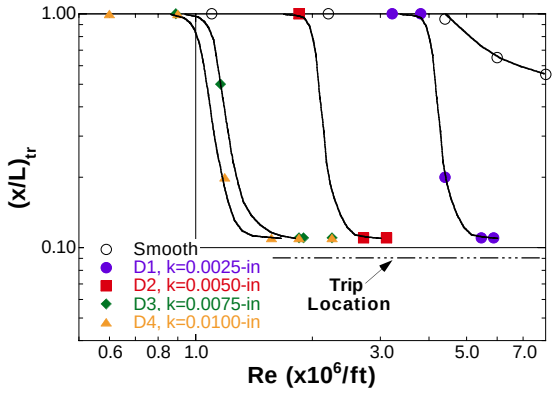

b) Station D

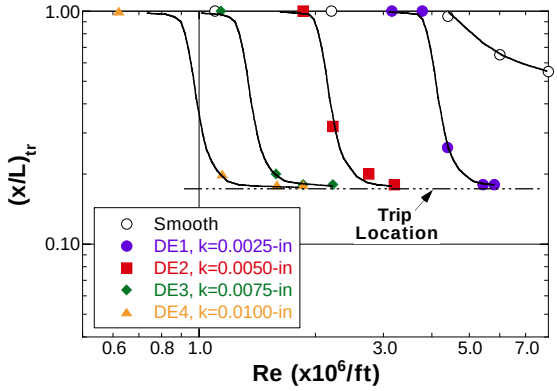

c) Station DE

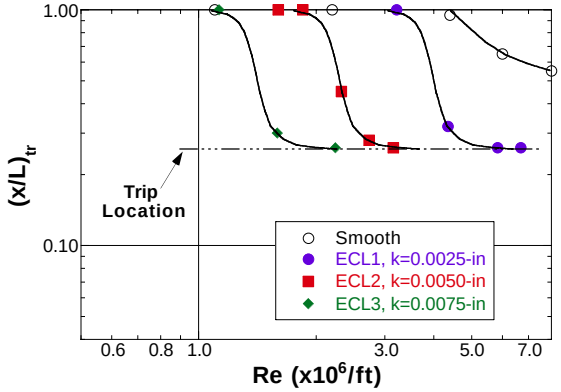

d) Station ECL

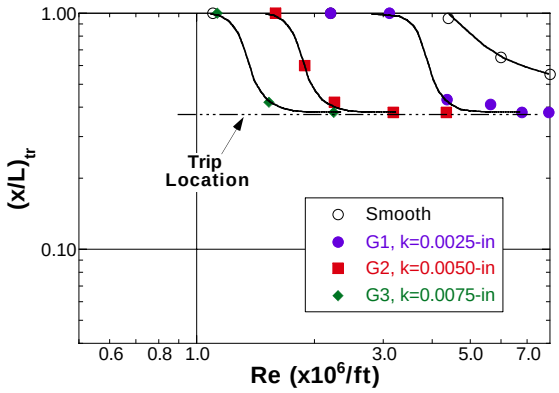

e) Station G

Fig. 10 Transition onset results along Orbiter centerline

Correlations

The primary objective of the present paper is to show the importance of using a consistent computational method when comparing different transition datasets. As stated earlier, Ref. 9 compared the Orbiter[3] and X-33[6] results but did not account for the different codes used to predict edge properties for those studies. Figure 15 presents the Orbiter effective transition data, recomputed with LATCH, as compared to the X-33[6] and X-38[7] results, using Re_θ/M_e as the transition parameter and k/δ as the disturbance parameter. The effective results of these three transition datasets are plotted in log-log coordinates, in a manner consistent with Ref. 9, to show that the data mostly falls within ±20% of a straight line representation of the power-law curve $(Re_\theta/M_e)(k/\delta)=70$. This result represents the ideal correlation where the data can be fitted by a power-law curve with a –45 degree slope (n = -1) and thus suggests a one to one dependence of transition parameter on the selected disturbance parameter. The selection of an uncertainty spread of ±20% of the curve fit was done to be consistent with the approach of Ref. 9. The key message from Fig. 11 is that when a consistent computational method is used, transition datasets that represent several different moderately blunt configurations at various angles-of-attack can be correlated using properties based on edge conditions. This fairly well behaved and simple correlation appears universally applicable to moderately blunt lifting body configurations in the same class of the Orbiter, as long as a consistent computational approach is used to apply the correlation.

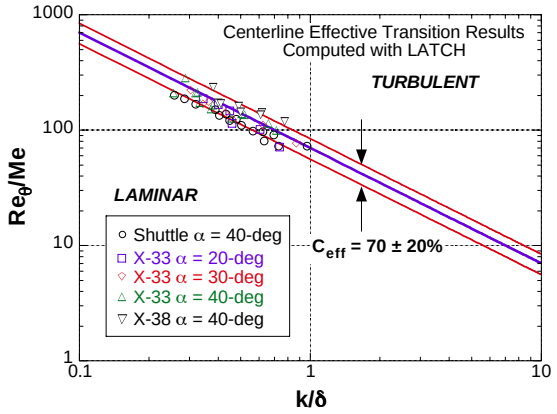

Fig. 11 Comparison of Orbiter effective data computed with LATCH to X-33 and X-38 results

The constant of 70 shown in Fig. 11 is roughly equivalent to the effective value for X-33 (60), published in Ref. 6. However, the approach used to generate the curve fit through the data for the X-33 program was slightly different, as the results were not represented by an average through the data, but rather as a conservative band within the incipient and effective trends. In other words, a constant of 60 represented the curve by which a majority (not just half) of the trips were shown to be fully effective. Further, in applying the X-33 roughness transition results to the flight vehicle design, an even more conservative approach was adopted where the incipient curve was used instead of the effective (in contrast to the results used in Ref. 9). As noted in Ref 6, the flight criterion of transition onset (Re_θ/M_e = 250 at x/L = 0.8 on centerline) corresponded to a k/δ = 0.2, based on the incipient curve. When this criterion was reached along the X-33 trajectory analysis, the entire vehicle was assumed to be turbulent. Also, these results were used to define the allowable roughness for the X-33 based on 0.2(δ) at the time of transition. It is the opinion of the present authors that until further flight transition data is obtained to help reduce uncertainties regarding the application of wind tunnel derived correlations to flight, conservative approaches, similar to what was used for the X-33 program, need to be adopted.

Figure 12 provides just the Orbiter results based on LATCH using the same transition and disturbance parameters as Fig. 11, but now including the incipient data. Both the incipient and effective trends are shown to fall within ±10% of the straight-line power-law curves of 36 and 55, respectively. By plotting these results with an uncertainty spread of ±10% (reduced from the ±20% used in Fig. 11), a well-behaved correlation is shown. The smooth model limit is shown, although a k/δ of 0.05 is the more appropriate value for this limit.

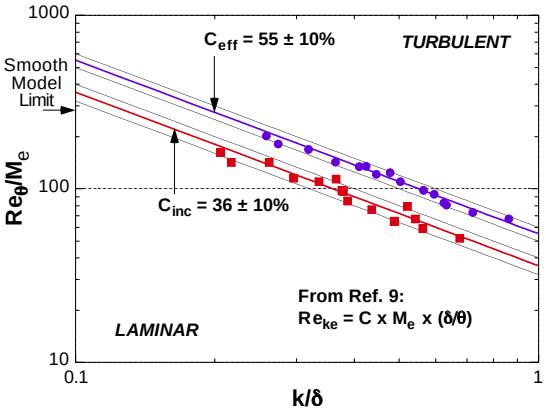

Fig. 12 Re_θ/M_e vs. k/δ for the Orbiter

Proponents of the Re_k approach have suggested that discrete roughness results can be related to distributed results based on the effective values for discrete.[9] However, the appropriateness of using the effective value for discrete for a comparison to distributed seems questionable. By definition for the distributed case, the critical roughness Reynolds number corresponds to the location of transition onset even though there may be a substantial run of distributed roughness prior. For the discrete case, the effective value of transition corresponds to when transition onset and the trip location are identical (or nearly so). If a second trip located ahead of the effective becomes prominent enough to be incipient, then conceivably transition onset could be promoted at the same location as that effective trip. As noted in Ref. 11, which discusses proposed trips for slender blunted cone configurations, when multiple trips (analogous to distributed) have been tested, the results were similar to when a single trip was placed at the location of the initial trip. This would suggest that the transition process is dominated by the first significant trip and not the interaction of the multiple trips. Therefore, a better comparison would be to use the incipient value for discrete and the critical value for distributed, especially in light of the previous discussion regarding conservative approaches. Reference 9 discusses the algebraic manipulation of the power-law relation shown in Fig. 12 to obtain a roughness Reynolds number based on local conditions (Re_{ke}) that is equal to the curve constant C times the edge Mach number (M_e) times the shape factor (δ/θ). Based on the incipient

curve of 36, M_e = 1.2, and δ/θ = 5.5, Re_{ke} = 240 is obtained, which is significantly different from the Orbiter value used in Ref. 9 (450 based on BLIMP).

Figure 13 provides the present Orbiter results computed with LATCH using Re_θ/M_e for the transition parameter and k/θ for the disturbance parameter. Both the incipient and effective trends fall within ±10% of the straight-line power-law curves of 200 and 310, respectively. Again, by using an uncertainty spread of ±10%, a well-behaved correlation is indicated. A similar algebraic manipulation of the relation shown in Fig. 13 provides $Re_{ke} = C(M_e)$. Using the incipient curve of 200 and M_e = 1.2 yields Re_{ke} = 240. The similarity in results between these two plots should not be surprising considering that LATCH computes the boundary layer thickness based solely on the shape factor, which would simply shift the results between the two figures. In hindsight, knowing that δ is not directly calculated, but instead uses an engineering relation perhaps more appropriate for flight, the correlation approach of Fig. 13 might have been preferable for X-33 and X-38, rather than Fig. 12. Again, the smooth model limit is shown (but is not implied to be at k/θ = 1).

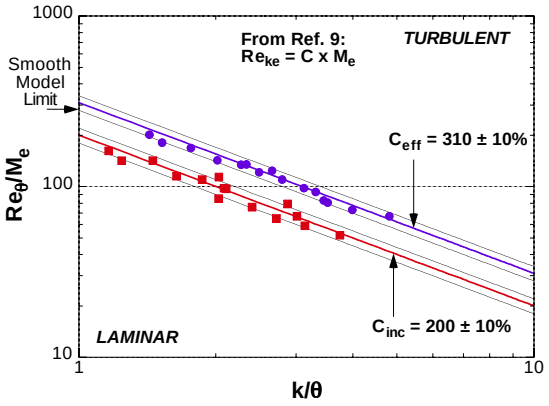

Fig. 13 Re_θ/M_e vs. k/θ for the Orbiter

In Fig. 14, Re_θ is plotted as a function of Re_k/Re_θ, as suggested by Ref. 9 (Re_θ is used as the transition parameter and Re_k/Re_θ is used as the disturbance parameter). Both the incipient and effective trends are shown with straight-line power-law curves of 140 and 250, respectively. In this case, the uncertainty spread of ±10% does not capture all the data, indicating a less well-behaved correlation. In fact the slope of the data appears to follow a trend whose curve would have an exponent of –0.7, which coincidentally is the same exponent used with the PANT correlation.[34] The incipient straight line curve shown (exponent of 1) provides a roughness Reynolds number (Re_k) of 140. Using the Re_k and Re_{ke} values obtained from the present investigation, based on incipient curves and the LATCH and SABLE computations, provides values roughly half those presented in Ref. 9. For comparison, if the effective curves had been used, the Re_k and Re_{ke} values would still have been 25% lower than Ref. 9. This result indicates the sensitivity of correlating approaches to the assumptions and codes used, and emphasizes the risk of comparing results from different studies without carefully considering what computational method was used.

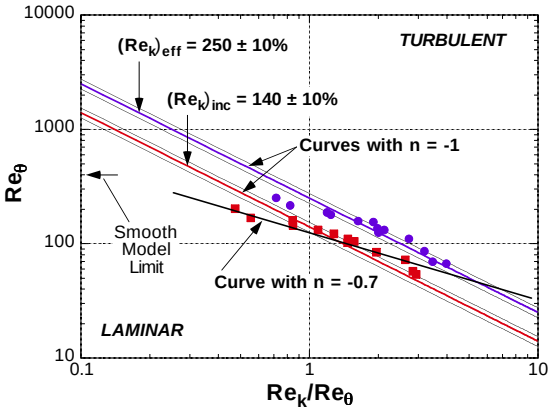

Fig. 14 Re_θ vs. Re_k/Re_θ for the Orbiter

The preceding results show that when a consistent computational method is used, a simple correlation based on edge conditions can be used to predict transition in the wind tunnel over the entire windward surface for several configurations at various angles of attack. Qualitatively, it also appears that these methods can be used to predict transition behavior on the Orbiter in flight.[4] This will be of interest to vehicle designers who tend to use simple approximate methods, such as the Miniver[16] code, to compute convective heating rates and edge conditions for predicting transition onset along proposed trajectories. The transition onset results provided in the present paper can thus be used to generate the appropriate correlation curve based on the preferred computational method of the designer. The use of incipient curves will instill some built-in conservatism until such time that detailed flight data can be obtained to quantitatively define transition onset as a function of a known trip height. Existing distributed roughness data can be used to define the smooth model limit, especially in the region of the stagnation point where the boundary layer is still sub-sonic.

Conclusions

Results from a previous experimental investigation of discrete roughness transition on the Shuttle Orbiter performed in the NASA LaRC 20-Inch Mach 6 Air Tunnel has been reanalyzed. Phosphor thermography was used to provide global heating images of the windward surface and to assess the state of the boundary layer. The discrete roughness elements were systematically varied in size and location along the model centerline for an angle of attack of 40 deg. The resulting roughness transition results were recomputed with the LATCH code and compared to X-33 and X-38 results (which were also computed using LATCH). The comparison showed that when a consistent approach is used, transition datasets, representing several configurations at various angles of attack, collapse into a well-behaved correlation based on edge properties.

Acknowledgements

The assistance of Stan Bouslog in providing additional BLIMP results for comparison to the present computations and many hours of consultation is greatly appreciated. Also, the reviews of the present paper by Steve Schneider, Vince Zoby, and Charles Miller certainly added much to the final product.

References

1. Haney, J. W., "Orbiter (Pre STS-1) Aeroheating Design Data Base Development Methodology: Comparison of Wind Tunnel and Flight Test Data," NASA CP-3248, *Orbiter Experiments (OEX) Aerothermodynamics Symposium*, April 1995, pp. 607-675.

2. Bouslog, S. A., An, M. Y., and Derry, S. M., "Orbiter Windward Surface Boundary Layer Transition Flight Data," NASA CP-3248, *Orbiter Experiments (OEX) Aerothermodynamics Symposium*, April 1995, pp. 703-739.

3. Berry, S. A., Bouslog, S. A., Brauckmann, G. J., and Caram, J. M., "Shuttle Orbiter Experimental Boundary-Layer Transition Results with Isolated Roughness," *Journal of Spacecraft and Rockets*, Vol. 35, No. 3, 1998, pp. 241-248.

4. Bouslog, S. A., Bertin, J. J., Berry, S. A., and Caram, J. M., "Isolated Roughness Induced Boundary-Layer Transition: Shuttle Orbiter Ground Tests and Flight Experience," AIAA Paper 97-0274, Jan. 1997.

5. Murray, A. L. "Further Enhancements of the BLIMP Computer Code and User's Guide," AFWAL-TR-3010, Wright-Patterson Air Force Base, OH, June 30, 1988.

6. Berry, S. A., Horvath, T. J., Hollis, B. R., Thompson, R. A., and Hamilton, H. H., "X-33 Hypersonic Boundary Layer Transition," *Journal of Spacecraft and Rockets*, Vol. 38, No. 5, 2001, pp. 646-657 (see also AIAA Paper 99-3560, June 1999).

7. Horvath, T. J., Berry, S. A., Merski, N. R., Fitzgerald, S. M., "X-38 Experimental Aerothermodynamics," AIAA Paper 2000-2685, June 2000.

8. Hamilton, H. H. II, Greene, F. A., DeJarnette, F. R., "Approximate Method for Calculating Heating Rates on Three-Dimensional Vehicles," *Journal of Spacecraft and Rockets*, Vol. 31, No. 3, 1994, pp. 345-354.

9. Reda, D. C., "Review and Synthesis of Roughness-Dominated Transition Correlations for Reetry Applications," *Journal of Spacecraft and Rockets*, Vol. 39, No. 2, 2002, pp. 161-167.

10. Stetson, K. F., "Comments on Hypersonic Boundary-Layer Transition," U.S. Air Force Wright Research and Development Center, WRDC-TR-90-3057, Sept. 1990.

11. Crusciel, G. T., "Active and Passive Boundary Layer Tripping,," AIAA 97-2016, June 1997.

12. Bouslog, S. A., An, M. Y., Campbell, C. H., Wang, K. C., and Pelley, R. L., "Orbiter Boundary-Layer Transition Working Group: Analysis and Ground Test Status Report," NASA Johnson Space Center, JSC-26812, Oct. 1994.

13. Batt, R. G., and Legner, H. H., "A Review of Roughness-Induced Nosetip Transition," AIAA J., Vol. 21, No. 1, Jan. 1983, pp.7-22.

14. Van Driest, E. R., and Blummer, C. B., "Boundary Layer Transition on Cones and Spheres at Supersonic Speeds – Effects of Roughness and Cooling," U.S. Air Force Office of Scientific Research, Rept. 67-2048, July 1967.

15. Berkowitz, A. M., Kyriss, C. L., and Martellucci, A., "Boundary Layer Transition Flight Test Observations," AIAA Paper 77-125, Jan. 1977.

16. Engel, C. D., and Praharaj, S. C., "Miniver Upgrade for the AVID System, Vol. I: LANMIN User's Manual," NASA CR-172212, Aug. 1983.

17. Miller, C. G., "Langley Hypersonic Aerodynamic/ Aerothermodynamic Testing Capabilities - Present and Future," AIAA Paper 90-1376, June 1990.

18. Merski, N. R., "Reduction and Analysis of Phosphor Thermography Data With the IHEAT Software Package," AIAA Paper 98-0712, Jan. 1998.

19. Buck, G. M., "Automated Thermal Mapping Techniques Using Chromatic Image Analysis," NASA TM 101554, April 1989.

20. Buck, G. M., "Surface Temperature/Heat Transfer Measurement Using A Quantitative Phosphor Thermography System," AIAA Paper 91-0064, Jan. 1991.

21. Micol, J. R., "Aerothermodynamic Measurement and Prediction for a Modified Orbiter at Mach 6 and 10 in Air," *Journal of Spacecraft and Rockets*, Vol. 32, No. 5, 1995, pp. 737-748.

22. Hollis, B. R., Horvath, T. J., Berry, S. A., Hamilton, H. H., and Alter S. A., "X-33 Computational Aeroheating Predictions and Comparisons with Experimental Data," *Journal of Spacecraft and Rockets*, Vol. 38, No. 5, 2001, pp. 658-669 (see also AIAA Paper 99-3559, June 1999).

23. Loomis, M. P., Venkatapathy, E., Davies, C. B., Campbell, C. H., Berry, S. A., Horvath, T. J., and Merski, N. R., "Aerothermal CFD Validation and Prediction for the X-38 Program," AIAA Paper 97-2484, June 1997.

24. Buck, G. M. and Vasquez, P., "An Investment Ceramic Slip-Casting Technique for Net-Form, Precision, Detailed Casting of Ceramic Models," U. S. Patent 5,266,252, November 30, 1993.

25. Bertin, J. J., Stetson, K. F., Bouslog, S. A., and Caram, J. M., "Effect of Isolated Roughness Elements on Boundary-Layer Transition for Shuttle Orbiter," *Journal of Spacecraft and Rockets*, Vol. 34, No. 4, 1997, pp. 426-436.

26. Bertin, J. J., Hayden, T. E., and Goodrich, W. D., "Shuttle Boundary-Layer Transition Due to Distributed Roughness and Surface Cooling," *Journal of Spacecraft and Rockets*, Vol. 19, No. 5, 1982, pp. 389-396.

27. Boudreau, A. H., "Artificially Induced Boundary-Layer Transition on Blunt-Slender Cones at Hypersonic Speeds," *Journal of Spacecraft and Rockets*, Vol. 16, No. 4, 1979, pp. 245-251.

28. Pate, S. R., "Dominance of Radiated Aerodynamic Noise on Boundary-Layer Transition in Supersonic-Hypersonic Wind Tunnels," Arnold Engineering Development Center, TR-77-107, Arnold Air Force Station, TN, March 1978.

29. Fay, J. A., and Ridell, F. R., "Theory of Stagnation Point Heat Transfer in Dissociated Air," *Journal of Aeronautical Sciences*, Vol. 25, No. 2, 1958.

30. Gnoffo, P. A., "An Upwind-Biased, Point-Implicit Relaxation Algorithim for Viscous, Compressible Perfect-Gas Flow," NASA TP-2953, Feb. 1990.

31. Anderson, J. D., Jr., *Hypersonic and High Temperature Gas Dynamics*, McGraw-Hill, New York, 1989, pg. 296.

32. Hamilton, H. H. II, Millman, D. R., and Greendyke, R. B., "Finite-Difference Solution for Laminar or Turbulent Boundary Layer Flow Over Axisymmetric Bodies With Ideal Gas, CF_4, or Equilibrium Air Chemistry," NASA TP-3271, Dec. 1992.

33. Zoby, E. V., Moss, J. N., and Sutton, K., "Approximate Convective-Heating Equations for Hypersonic Flows," *Journal of Spacecraft and Rockets*, Vol. 18, No. 1, 1981, pp. 64-70.

34. Stetson, K. F., "Boundary-Layer Transition on Blunt Configurations," NASA Johnson Space Center, JSC-26528, Feb. 1994.

Table 1: Fiducial marks and trip locations.

Trip	x/L	y/L
A	0.050	0.00
B	0.070	0.00
C	0.070	0.011
D	0.090	0.00
DE	0.0174	0.00
ECL	0.258	0.00
E	0.258	0.015
F	0.258	0.039
G	0.375	0.00
H	0.375	0.033
I	0.375	0.053
J	0.575	0.00
K	0.620	0.133

Table 2: Nominal flow conditions and run-to-run repeatability for 20-Inch Mach 6 Air Tunnel.

$Re_\infty(x10^6/ft)$	M_∞	P_{t1} (psi)	T_{t1} (°R)	H_{t1}(BTU/lbm)	P_{t2}(psi)
0.59±4.6%	5.84±0.03%	29.8±4.4%	861.7±0.3%	207.2±0.3%	0.99±4.2
0.88±2.1%	5.86±0.03%	44.8±2.9%	865.9±0.9%	208.2±1.0%	1.47±2.8
1.15±3.3%	5.88±0.05%	60.3±3.8%	880.8±0.5%	212.0±0.5%	1.95±3.7
1.58±2.6%	5.90±0.03%	84.7±2.4%	889.7±0.8%	214.2±0.8%	2.69±2.2
1.86±1.7%	5.92±0.03%	100.1±2.2%	887.6±0.3%	213.5±0.7%	3.14±2.1
2.23±1.8%	5.94±0.02%	125.1±1.4%	906.7±0.7%	218.2±0.7%	3.88±1.3
2.73±1.7%	5.95±0.01%	154.7±1.0%	909.1±0.5%	218.8±0.5%	4.74±0.9
3.16±2.4%	5.96±0.02%	180.3±1.6%	909.9±0.8%	219.0±0.9%	5.48±1.5
3.79±0.8%	5.98±0.00%	217.0±0.1%	909.1±0.5%	218.8±0.5%	6.54±0.1
4.40±2.3%	5.98±0.01%	250.7±1.1%	906.2±1.0%	218.1±1.1%	7.52±1.1
4.87±3.2%	5.99±0.01%	292.2±0.7%	933.3±1.5%	224.8±1.6%	8.73±0.7
5.41±1.6%	6.00±0.01%	325.6±0.6%	934.1±0.9%	225.0±0.9%	9.69±0.6
5.81±3.0%	6.00±0.03%	348.7±3.0%	931.8±0.5%	224.4±0.5%	10.35±2.9
6.73±1.8%	6.01±0.02%	401.7±1.4%	926.6±0.4%	223.1±0.4%	11.85±1.3
7.95	6.02	475	925	222.6	13.88

Table 3: Orbiter incipient roughness results at α = 40 deg in the LaRC 20-Inch Mach 6 Air Tunnel.

Trips	Re_{inc}	θ	δ	Re_θ	Re_θ/M_e	Re_k
B2	1.6	0.00166	0.00923	57	67	163
D1	3.8	0.00123	0.00685	105	114	165
D2	1.9	0.00174	0.00960	72	79	189
D3	1.0	0.00239	0.01330	54	59	158
D4	0.8	0.00267	0.01478	48	52	
DE1	3.8	0.00172	0.00954	160	142	135
DE2	1.9	0.00240	0.01330	110	98	162
DE3	1.1	0.00312	0.01720	84	76	165
DE4	0.8	0.00368	0.02049	73	65	
ECL1	3.1	0.00201	0.01153	168	142	93
ECL2	1.9	0.00268	0.01490	132	110	144
ECL3	1.1	0.00370	0.01937	102	85	150
G1	3.1	0.00215	0.01215	203	162	96
G2	1.6	0.00305	0.01690	144	115	122
G3	1.1	0.00356	0.01980	122	97	156

Table 4: Orbiter effective roughness results at α = 40 deg in the LaRC 20-Inch Mach 6 Air Tunnel.

Trips	Re_{eff}	θ	δ	Re_θ	Re_θ/M_e	Re_k
B2	2.2	0.00142	0.00791	70	80	241
D1	5.2	0.00107	0.00590	125	135	250
D2	2.5	0.00151	0.00840	86	93	274
D3	1.6	0.00188	0.01040	67	73	265
D4	1.3	0.00208	0.01160	62	67	
DE1	5.4	0.00142	0.00785	188	168	224
DE2	2.7	0.00201	0.01120	136	121	270
DE3	1.9	0.00240	0.01330	110	98	299
DE4	1.3	0.00290	0.01603	93	83	
ECL1	5.0	0.00164	0.00913	216	181	178
ECL2	2.8	0.00220	0.01220	158	134	258
ECL3	1.8	0.00268	0.01490	132	110	280
G1	4.8	0.00175	0.00969	252	201	180
G2	2.4	0.00248	0.01374	179	143	222
G3	1.8	0.00282	0.01570	155	124	295